ELSEVIER

Journal of Nuclear Materials 240 (1997) 241–250

journal of nuclear materials

Kinetics and mechanisms of the reaction of air with nuclear grade graphites: IG-110

E. Loren Fuller [*,1], Joseph M. Okoh [2]

Carbon Materials Technology Group, Metals and Ceramics Division, Oak Ridge National Laboratory, Oak Ridge, TN 37831-6088, USA

Received 15 April 1996; accepted 25 July 1996

Abstract

The work presented in this report is part of an ongoing effort in the microgravimetric evaluation of the intrinsic reaction parameters for air reactions with graphite over the temperature range of 450 to 750°C. Earlier work in this laboratory addressed the oxidation/etching of H-451 graphite by oxygen and steam. This report addresses the air oxidation of the Japanese formulated material, IG-110. Fractal analysis showed that each cylinder was remarkably smooth, with an average value, D, the fractal dimension of 0.895. The activation energy, E_a, was determined to be 187.89 kJ/mol indicative of reactions occurring in the zone II kinetic regime and as a result of the porous nature of the cylinders. IG-110 is a microporous solid. The low initial reaction rate of 9.8×10^{-5} at 0% burn-off and the high value (764.9) of Φ, the structural parameter confirm this. The maximum rate, 1.35×10^{-3} g/m^{2}s, was measured at 34% burn-off. Reactions appeared to proceed in three stages and transition between them was smooth over the temperature range investigated. Both E_a and ln A did not vary with burn-off. The value of ΔS, the entropy of activation, was -41.4 eu, suggesting oxygen adsorption through an immobile transition state complex. Additional work is recommended to validate the predictions that will be made in relation to accident scenarios for reactors such as the modular high temperature gas-cooled reactor where fine grained graphites such as IG-110 could be used in structural applications.

1. Introduction

1.1. Rationale

Graphite is an effective nuclear moderator for use in high temperature gas cooled reactors (HTGR). The core-moderator region, reflector and core support posts of the modular high temperature gas-cooled reactor (MHTGR) are manufactured from nuclear grade graphite [1]. In light of this important application, the chemistry of graphite has always aroused keen interest.

The kinetic and thermodynamic studies described in this paper are part of an ongoing program to accomplish the following objectives: (i) add more relevant chemical kinetic and thermodynamic data to the available data base to facilitate reactor design, (ii) provide a solid basis for an improved understanding of the reaction mechanism involved in the air oxidation of graphite, (iii) model air-ingress scenarios, reaction rates and mechanisms due to the air exposure of nuclear grade graphite.

Earlier work in this laboratory addressed graphite oxidation/etching by steam, and carbon dioxide [2,3]. Oxidation by dry breathing air is the subject matter of this study. Excessive air corrosion of nuclear reactor graphite can compromise the structural integrity of the fueled graphite block which comprises the core moderator region. For example, a 50% reduction in tensile strength has been measured for a 7% burn-off and a factor of 2 reduction in compressive strength has been reported at 10% burn-off [4]. Such compromises will raise investment risk to unacceptable margins. Consequently, the rationale is to define conditions, from the chemical point of view, for the design of an efficient and safe nuclear reactor.

* Corresponding author.

[1] Department of Geological Sciences, The University of Tennessee, Knoxville, TN, USA.

[2] Department of Natural Sciences, University of Maryland Eastern Shore, Princess Anne, MD 21853, USA.

PII S0022-3115(96)00462-X

1.2. Background

1.2.1. Reaction equations

Reactions of other graphites with the normal constituents of air have been studied in detail [2,3]:

$$C(\text{solid}) + O_2(\text{gas}) \rightarrow CO_2(\text{gas}) \quad \Delta H = -393.4\ \text{kJ/mol}, \tag{1}$$

$$C(\text{solid}) + H_2O(\text{gas}) \rightarrow 2CO(\text{gas}) + H_2(\text{gas}) \quad \Delta H = +130.3\ \text{kJ/mol}, \tag{2}$$

$$C(\text{solid}) + CO_2(\text{gas}) \rightarrow 2CO(\text{gas}) \quad \Delta H = +170.7\ \text{kJ/mol}, \tag{3}$$

$$C(\text{solid}) + 2H_2(\text{gas}) \rightarrow CH_4(\text{gas}) \quad \Delta H = -74.8\ \text{kJ/mol}. \tag{4}$$

These reactions may be of chemical or diffusion control, or both, in varying contributions. Our chosen reaction conditions are such that the rate is partially controlled by pore diffusion. This means that the gaseous reactant concentration falls gradually to zero at some point in the pore system of the graphite, putting the reaction into the Zone II kinetic regime, where the rate determining step becomes one of chemical control. Although air is mentioned as the reactant, it is the reaction with oxygen that is dominant, compared to carbon dioxide and steam. The relative reactivities of these gases are presented in Table 1 [5].

1.2.2. Morphology

Fuller et al. [2,3], in their accounts of the gasification of H-451 graphite, reported that the measured chemical control reaction rates are strongly dictated by substrate morphology and changes brought about by the reaction per se. The details of this morphology dependence, though only lightly considered in the current studies, will be investigated in the future.

The gasification rate of graphite increases with burn-off to a maximum value at 20–30% of complete burn-off and then decreased. According to Su and Perlmuter [6], this effect is attributable to an initial increase in reaction-surface area as the pore walls gasify. Later, the pore walls grow larger and join each other and the surface area decreases. The physical structure of the solid reactant, which changes continuously as the reaction proceeds, evolves pore structure and affects reaction kinetics by altering the availability of reaction surface area. To investigate this effect Eq. (5), developed in Ref. [6] which interprets conversion data and the changes of reaction surface area in terms of a combination of chemical and pore size effects, will be used to analyze our data. Their equation describes the reaction rate as

$$R_t/R_0 = S/S_0 = (1-X)\left[1 - \Phi \ln(1-X)\right]^{0.5}, \tag{5}$$

where the 'structural parameter' is defined as

$$\Phi = \left[4rI(1-p_t)L_0\right]/\left[d_t A_{\text{BET}}\right]^2 \tag{6}$$

and the porosity at time, t, is measured as

$$p_t = V_0/V_t - 1/d_t. \tag{7}$$

L_0 is the effective pore length per unit volume. A_{BET} is the BET surface area per unit mass of solid. d_t is the true density of porous graphite at time t. X = fractional burn-off. R_t and R_0 are reaction rates at time t and at 'time zero' corresponding to the reaction initiation.

Table 1
Comparison of reaction rates for gaseous reactions with solid graphitic carbon based (Ref. [5], 800°C and 0.1 atm)

Reaction	Relative rate
Oxygen gas plus carbon	10 000
Water vapor plus carbon	3
Carbon dioxide gas plus carbon	1
Hydrogen gas plus carbon	0.003

1.2.3. Fractal analysis

The geometry of the environment in which the chemical gasification reactions occur is an important consideration since factors like diffusional routes, rates, molecular ground state and excited state conformations, and the order of molecular electronic energy levels are affected by it [7]. The fractal dimension D, of a surface, is an intrinsic property which can be used to quantify the geometric characteristics or surface irregularity of an object. Conditions of D equal to 2 refers to the classical concept of smooth, flat areas; evaluated D values between two (2) and three (3) approximates surfaces of increasing roughness. The rate of a gas/solid reaction should be influenced by the surface fractal dimension when the accessibility of active sites or the surface is the rate determining factor [8]. The value of the fractal dimension, D, may be extracted from the rate equation [4]

$$R = k_i P^n t^h = Bt^h, \tag{8}$$

$$h = 1 - D/2, \tag{9}$$

where k_i, P^n and t are reaction rate constant, partial pressure of O_2 (raised to the power n, corresponding to the order of the reaction) and reaction time (measured in minutes for this study).

1.2.4. Kinetics and mechanism

The mechanism of graphite oxidation may be described by one of two models. In the first, a shrinking core model, the reaction occurs on the outside surface of individual particles and proceeds inward, leaving behind a layer of ash. In the other, the presence of a large number of pores, many of which are interconnected, permits oxidation to proceed within the material as well as on the outer surface [3,9]. Dimensional analysis of the graphite cylinders before

and after oxidation will suggest which of these two is applicable. The proposed models are predicated on the following consecutive elementary processes:

(i) diffusion of reactants to the surface,
(ii) adsorption of reactants at the surface,
(iii) chemical reaction on the surface and within pores,
(iv) desorption of products,
(v) diffusion of products away from the surface and pores.

With an adequately excess supply of reactant gases (adequate flow of carrier gas) one can ignore contributions of steps (i) and (iv), the activation energy of the gasification reaction may be dictated by (a) adsorption of reactant gas to form a reactive intermediate surface complex, (b) chemical reaction to form a surface chemical bond which in turn may or may not form a transient complex precursor to the reaction products, and (c) desorption of the product gas(es). The adsorption process may be considered as molecular involving an atom or a molecule from the gas phase and an active carbon on the graphite surface. The energy of activation required may be due to the activated complex which is formed between the molecule or atom and the active carbon atom. Desorption from an immobile layer involves an activated state in which a molecule attached to an adsorbing center acquires the proper configuration and activation energy to permit it to escape from that surface. Literature reports [10] suggest that the activation energy of the chemical reaction component is dependent on the level of impurity in the sample. For example, $E_a = 251$ kJ/mol at 5 ppm and $E_a = 168$–189 kJ/mol at 150 ppm total impurity content in the sample. This observation might be significant since the level of impurity, which might have been as low as 5 ppm at zero burn-off, may gradually increase during oxidation to 0.5% at 75% burn-off. Some authors have proposed that two parallel reactions occur on the graphite surface [11]. One of these with an activation energy of about 251 kJ/mol takes place on the clean graphite surface and the other with an activation energy of 147–159 kJ/mol on the contaminated surface. Generally, the more contaminated the graphite, the lower is the energy of activation. Another factor which has been proposed to determine the activation energy of the chemical reaction component is the product ratio of $CO:CO_2$. The individual activation energies for the formation of the two primary products, CO and CO_2 are 60–62 and 58–60 kcal/mol, respectively, and the overall reaction activation energy will depend on which is predominant. From the above, an inverse relationship between the activation energy, E_a, and the CO/CO_2 ratio, r, will be clarified in the discussions of our results.

The reaction rate (R) can be evaluated in terms of the rate of mass lost [3,12]:

$$R = \mathrm{d}m/\mathrm{d}t = k_{air} S P^n, \tag{10}$$

where k_{air} is the reaction rate coefficient, P is the pressure of the reacting breathing air, n is the reaction order and S the surface area. The equation above is based on the rate law proposed by Hinshelwood

$$R = -\mathrm{d}m/\mathrm{d}t = \frac{k_{air} S P^n}{\left(1 + k' P^p(\mathrm{CO}) + k'' P^q(\mathrm{CO_2})\right)} \tag{11}$$

for the reaction between a porous solid and gas. In the present case we are assuming that $1 \gg \{k' P^p(\mathrm{CO}) + k'' P^n(\mathrm{CO_2})\}$ due to the rapid flow of carrier gas, minimizing the concentration of the product gases in the environs of the carbon surface.

In order to compare our data with literature values, the rate law [13]

$$K_o = k_{mc}(m_a P_o)^n \tag{12}$$

in the units of g/g h will be used.

$$k_{mc} = K_o/(m_a P_o)^n \tag{13}$$

where m_a is the mole fraction of reacting gas, P_o is the total pressure, K_o is the reaction ratio and k_{mc} the rate constant. We shall convert our rates in mg/min to $g/m^2 s$ by using theoretically calculated active surface area, assuming 15.6 μg of active carbon per gram of graphite [14] and a cross-sectional area of 8.3 $Å^2$ per atom of carbon [15].

The temperature dependence of graphite gasification will be evaluated from the Arrhenius equation:

$$k = A e^{-Ea/RT}, \tag{14}$$

where k is the rate constant, R is the universal gas constant and T is the reaction temperature.

The use of this equation will enable us to calculate the respective values of the energy (E_a), entropy (ΔS), enthalpy (ΔH) of activation and the frequency factor A. By using the absolute rate theory, a theoretical value of the frequency factor will be obtained from the equation

$$A = (k_B T/h) f^*/f_a, \tag{15}$$

where k_B is the Boltzmann constant, T is the absolute temperature, h is Planck's constant, and f^* and f_a are the partition functions of the transition state complex and the adsorbed species, respectively. The values of A will be compared with those that have been reported in the literature [16–18].

2. Experimental

2.1. Graphite samples

The graphite cylinders used in this study were supplied by the Japan Atomic Energy Research Institute (JAERI), and were machined from Toyo Tanso grade IG-110, which is an isostatically molded, isotropic, fine-grained, halogen purified nuclear-grade graphite. This halogen treatment decreases the silicon content of the material, making it

Table 2
Lot analysis record for breathing quality air compressed from atmosphere, CGA grade E (Lot #23345690)

Carbon monoxide	2 ppm
Carbon dioxide	400 ppm
Nitrogen oxides	not detected
Sulfur dioxide	not detected
Water vapor	0.05 ppm
Total hydrocarbons	2.5 ppm
Oxygen (by test)	21%
Odor	not detected
Oil	not detected

potentially more reactive than H451, K018 and K022 [2,3]. Samples were machined to cylindrical specifications: diameter 0.838 cm and length 1.905 cm. Prior to analyses samples weighed 1.756 ± 0.002 g (Mettler Model AT261, Delta Range) reflecting the macroscopic uniformity of the samples supplied for analyses. Sample dimensions were individually measured and recorded utilizing electronic digital calipers (Model 950-201 MAX-6). White cotton gloves were worn whenever cylinders were handled.

2.2. Apparatus

A recording vacuum thermoanalyzer (Mettler Instruments Model TAl Serial #61) equipped with a Honeywell 16 channel DPR 3000 250 mm strip chart recorder was used for thermogravimetric analyses. The crucible and crucible support rod were made of alumina with the crucible support rod equipped with Pt/Rh(l0%)–Pt thermocouple elements. Weights were measurable to within ± 0.5 mg precision. Temperature regulation and programmable temperature ramps are determinable to within ± 1.5 and ± 0.5°C accuracy, respectively. An environmental chamber with associated flow gauges and controllers which can operate from vacuum to atmospheric pressures, encases the beam balance of the weighing system. Appropriate tare weights are applied for gross taring, with servoelectric balance maintained continuously. When mounted, the sample rests above the beam in a furnace that can attain temperatures of up to 1600°C. The reactant gas, dry breathing air compressed from the atmosphere, CGA grade E, was supplied from lots #562071591A for runs J001 to J004 and #23345690C for runs J005 to J009. A typical analysis of these air samples is presented in Table 2. The air flow rate for each run varied between 0.496 and 0.500 standard liters per minute (SLPM). A Bausch and Lomb microscope was used for visual observations at linear magnifications of up to $30\times$. The microscope equipped with a camera (32 mm MicroTessar Lens) was used to photograph the graphite cylinders for the purpose of dimensional comparison.

2.3. Procedure

The selection of the samples used were randomized. Taring was done with and without air flow without any observable effects. At the chosen air flow rate (0.496–0.500 SLPM) and reaction temperatures (450–750°C) diffusional mass transport effects were minimized. For a desired burn-off, the sample was quickly heated to 750°C and the temperature held constant. In order to determine the activation energy of the reaction each graphite cylinder was heated to 750°C. The reaction temperature was then reduced to 700, 650, 600, 550, 500, and 450°C successively. The time required and the incremental weight loss were kept to a minimum as reaction rates change significantly with different degrees of burn-off. Data were collected for each run as a continuous record of the sample mass, temperature and time derivative of the sample mass.

3. Results and discussion

3.1. Morphology

Table 3 presents the dimensions of separate IG-110 samples before and after a specified burn-off. Although mass loss was noted continuously, no pronounced changes in dimensions were observed prior to 42.62% burn-off. After its attainment, changes became more pronounced. For example, changes in dimensions at 42.62% burn-off were -0.031 cm (O.D.), with no change in length. The changes in dimensions at 53.88 and 62.83% burn-offs were -0.061 cm (O.D.) and 0.107 cm (1) and 0.094 cm (O.D.) and 0.079 cm (1), respectively. These results suggest that oxidation proceeds within the graphite cylinders initially with little or no decrease in macroscopic change in sample size. A more detailed study of the morphology of the samples, using scanning electron microscopy is needed for confirmation and to enable a closer examination of the surface and pore structure as they evolve during oxidation. Visual observations at up to $5\times$ magnification, showed that the surface of the oxidized cylinders became 'grainy' during reaction. Initial mass loss appeared to occur through

Table 3
Dimensional analysis of IG-110 graphite cylinders before and after oxidation in air

Burn-off (%)	Length (cm)			Diameter (cm)		
	initial	final	change	initial	final	change
5.7	1.905	1.905	0.000	0.841	0.833	−0.008
13.30	1.902	1.905	0.003	0.841	0.831	−0.010
25.29	1.905	1.902	−0.003	0.841	0.823	−0.018
42.62	1.905	1.905	0.000	0.841	0.810	−0.031
53.88	1.902	1.795	−0.107	0.838	0.777	−0.031
62.83	1.905	1.826	−0.079	0.841	0.747	−0.094

internal chemical etching with external physical dimensional loss at higher degrees of burn-off.

3.2. Effect of reaction time on oxidation

The physical processes which control the oxidation of porous graphite blocks are boundary layer transport, in-pore transport and chemical reaction kinetics. At sufficiently low temperatures (450–750°C), as used in this study, air permeation tends to occur quickly throughout the porous graphite cylinders and the reaction becomes one of chemical control. However, it appears that the availability of reactive surface area regulates reaction rate.

Our first indication of this effect was reflected in the spacing of the lines which represent the highly expanded mass scale in the TGA strip chart. Using a typical run (J001) at 750°C and 81.15% burn-off, the spacing between them went through a minimum in mid-reaction, compared to the beginning and end stages. Fig. 1, for example, shows the continuous change with elapsed oxidation time, of the directly measured weight loss, from run J004. As implied by the sigmoidal nature of the resulting curve, the oxidation may be considered to proceed in three stages, reflecting variations in an intrinsic property of the samples that were used.

In Fig. 2(a), reaction rates that were measured at different burn-offs at 750°C are plotted as a function of fractional burn-off, using a different graphite cylinder for each datum. A maximum in the measured rates of 8.545 mg/min (95% confidence level), which decreased to zero at 100%, occurred at 42.62% burn-off. In order to confirm the observation above, a graphite cylinder was gasified at 750°C, and reaction rates were again measured at ~ 5, 9.84, 24.42, 41.14, 55, 63.89, 75.91, 81.44, and 87.75% burn-off. The curve which results from the plot of the measured rates as a function of burn-off is shown in Fig. 2(b). Despite some few differences, the general agreement between the sets of data presented in Fig. 2(a) and (b) establishes the uniformity in the chemical and physical properties of the graphite cylinders that were used in the, present work. Reports in literature for the gasification of coal char and graphite in air show that the surface area generated goes through a maximum at $\sim 40\%$ and 50% burn-off, respectively. Consequently, it is our impression that the intrinsic property which controls gasification is the reactive surface area, the magnitude of which varies in the course of gasification.

3.3. Structural parameter, (Φ) / reaction surface area

Eq. (5) relates the reaction surface area to conversions in terms of pore structure and particle size parameters [6]. The Φ term can be used to quantify the porosity of graphite on which the magnitude of the reactive surface area depends [7]. The graph of R_t against the degree of consumption (burn-off on a mass basis) in Fig. 2(b).

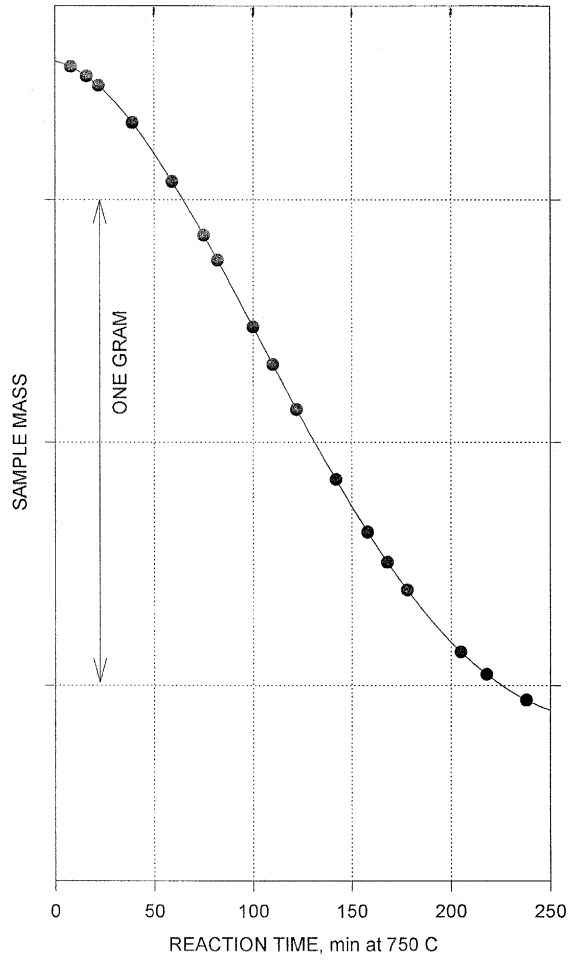

Fig. 1. Reaction data for the exposure of the graphite cylinders of IG-110 to air at 750°C. Sigmoidal curve reflects the successive stages of oxidation, 1. initiation of pores by etching, 2. increase of porosity within grains and binder, and 3. consumption of skeletal substrate residue.

According to this graph, a maximum in conversion rate occurs at 42.62% burn-off when the value of Φ is 764.9. A variety of studies on char gasification [19–21] demonstrate that measured reaction rates of gasification show a maximum at intermediate conversion level. The high value of Φ is indicative of the highest porosity attainable and consequently the highest reactive surface area presented for gasification at intermediate conversion. It has been proposed that this maximum arises from two opposing effects, the growth of reaction surfaces associated with the pores, and the loss of these surfaces as they progressively collapse by longitudinal intersection [6]. We are of the impression that the trends are attributable to the (1) initiation of porosity by an etching process, (2) growth lengthening of pores by the same etching mechanism, and (3) eventual collapse of macropores due to intersection and

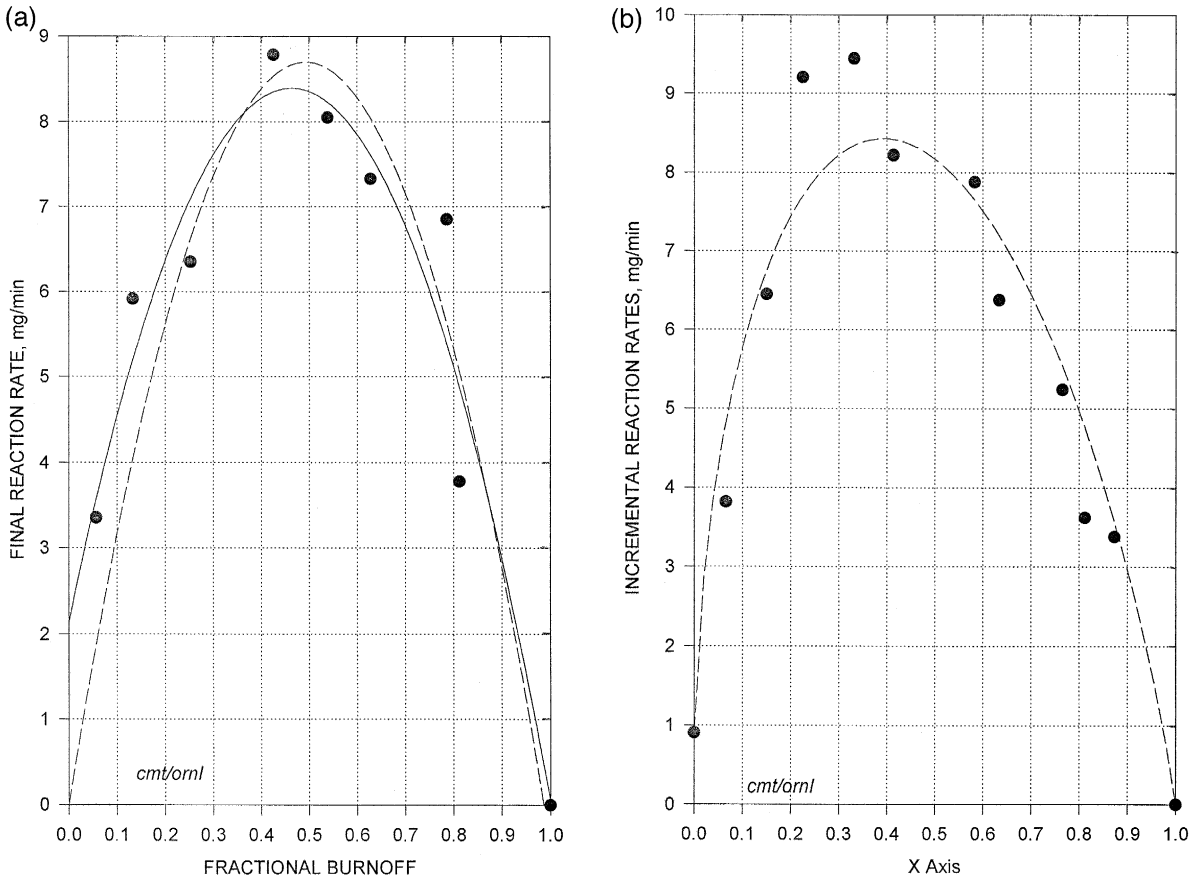

Fig. 2. (a) Reaction data for the exposure of the graphite cylinders of IG-110 to air at 750°C. Maximum rate of reaction is apparent at intermediate conversion ca. 38% burn-off. This data was acquired from different cylinders at different degrees of burn-off. (b) Reaction data for the exposure of IG-110 to air at 750°C. Maximum reaction rate of reaction is noted at 34% burn-off. This data was acquired from one graphite cylinder.

actual consumption of the substrate skeletal matrix material.

The results of a least squares fit of our data and those from previous runs using samples K018 and K022 are presented in Table 4. Some pertinent observations are noteworthy.

(1) The method of estimating the structural parameter presents a good means of evaluating the initial rates of the reaction. Of the three samples, IG-110 is the least reactive initially, as shown by the values: 9.81×10^{-5}, 4.35×10^{-4}, and 2.387×10^{-4} g/m^{2}s for IG-110, K022, and K018, respectively.

Table 4
Structural parameter (Φ) evaluation for air oxidation of nuclear graphites at 750°C. Data for K018 and K022 from Fuller et al. [3]

Sample	K018	K022	IG-110
Initial rate, R_o	1.65	3.01	0.68
Standard deviation	0.05	0.12	0.00
Structural parameter, Φ	128	377	765
Standard deviation	8.00	3.00	0.013
Overall correlation, R^2	0.996	0.985	0.999

(2) Regardless of the magnitude of Φ, the maximum rate (8 mg/min for the samples K018, K022, and 8.5 mg/min for IG-110) occurs at ~40% burn-off where it correspondingly attains it maximum value.

(3) Even though IG-110 is the least reactive initially, it presents the highest porosity or the largest surface area (i.e., highest Φ) when it attains maximum rate. This may not be surprising as it has been halogen purified, thus containing the lowest amounts of catalytic impurities (and incidentally silica which is known to be an oxidation retardant for graphitic carbons). Due to its lowest initial rate, one might conclude that IG-110 presents a very smooth surface compared to K018 and K022 initially, consisting most predominantly of micropores, after manufacture. This observation will be confirmed by fractal analysis. Their order of smoothness may be listed as: IG-110 > K018 > K022.

From the foregoing, one can reasonably infer that reactions occur in micropores where available surface area is low in the first stage of oxidation. In the second stage as gasification proceeds, closed pores are opened and micropores are converted to macropores or mesopores, leading to a very rapid increase in reactivity due to the generation of fresh additional surface area. This process opens the extremities of the bulk of the graphite cylinders to oxygen molecules and accelerates the oxidation process. Eventually the pore walls begin to be consumed and the reactive surface area decreases. At $\sim 40\%$ burn-off where rate is maximum, the reactive surface area probably attains its maximum value due to the conversion and growth of micropores to macropores. When the consumption of pore wall commences and the surface area decreases, the rate declines. These contentions are supported by Fig. 1, and can be confirmed by measuring the residual surface area as a function of burn-off. Experiments are currently underway to estimate these intermediate surface areas by nitrogen adsorption at 77 K.

3.4. Fractal analyses / pore geometry

The geometry of the porous environment in which the reactions occur was determined from the graph of log R (mg/min) against log t (min) using a typical run (J004). Results are presented in Fig. 3. From the slope (0.5523), the value of D, the fractal dimension, is computed to be 0.895. $D = 1.230$ and 1.202 for K022 and K018, respectively. From the magnitudes of these values, one can conclude that the graphite cylinders of IG-110, K022 and K018 are microporous solids. By using the values of ln B, (-0.203, 0.166, and 0.076), respectively, the rate constants k_i at $t = 1$ min are: 1.181×10^{-4}, 1.708×10^{-4}, and 1.561×10^{-4} g/m^{2}s, respectively, for IG-110, K018 and K022, respectively. The calculated rates compare well to the literature values that are quoted in Table 5.

The fractal dimension D describes the surface roughness and the resistance to air flow within the pores in the course of gasification of the graphite cylinders that were used in our studies. Using the values of D (enclosed in parenthesis), we are led to conclude that the surface smoothness of these samples vary in the order: IG-110 (0.895) > K018 (1.202) > K022 (1.230), in agreement with the trend that was established by the structural parameter, Φ. It appears that this order is preserved during gasification as the highest attainable rates for the gasification process are 8.5 mg/min for IG-110 and 8.0 mg/min for K018 and K022.

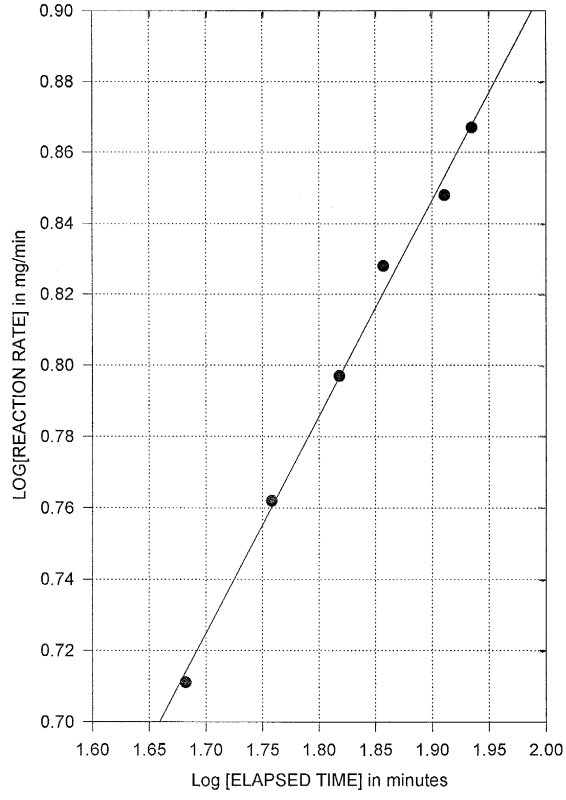

Fig. 3. Fractal analysis of the graphite cylinders of IG-110. Slope and intercept relate to initial roughness and topography generated by the reaction with oxygen in air.

Based on our results, a minimum in the various values of D as a function of degree of burn-off is expected at

Table 5
Representative literature survey of kinetic parameters for oxygen reaction with graphite

Rate ($\times 10^3$) (g/m^{2}s)	k ($\times 10^4$) (g/m^{2}s)	E_a (kJ/mol)	Citation	Reference
–	48	184	Laine et al.	[14]
1.5	14	176	Blyholder and Eyring	[22]
–	–	197	Hawtin et al.	[23]
0.27	–	–	Evans	[24]
0.398	–	–	Baker and Harris	[25]
–	–	190	Hawtin and Murdoch	[20]
–	0.019	–	Walker et al.	[26]
0.435	1.71	168	Fuller et al. H451(K022)	[3]
0.238	1.56	168	Fuller et al. H451(K018)	[3]
0.098	1.18	188	this work (Toyo Tanso, IG-110)	

approximately 40% burn-off. This minimum will correspond to the smoothest (least tortuous) surface presented by the pores for the passage of reactive air molecules. Observations from experiments in which D is measured at different degrees of activation using char, suggest these to be the case [27,28].

3.5. Kinetic considerations

At this juncture the values of the activation energies of gas–carbon reactions, where the rate is controlled solely by resistance to chemical reactivity, is of interest.

A typical plot of log R (reaction rate) against $1/T$ is shown in Fig. 4. The curve is linear with a slope of $E_a/R = 22.00$, $E_a = 187.89$ kJ/mol, and an intercept (ln A) of 24.17. Different values of E_a and ln A that were determined as described above are listed in Table 6. Within 95% level of confidence these remained constant with burn-off in the temperature range studied. In experiments where the air oxidation of H-451 was studied [2,3], the value of the activation energy E_a was 168 kJ/mol with the pre-exponential factor ln $A = 21.70$. For reactions in which rates depend on the diffusion of reactive gases through pores, the value of E_a is 187.9 kJ/mol [3]. The excellent agreement with our value confirms the porous nature of the graphite cylinders of IG-110 and that they were the site of the oxidation reactions.

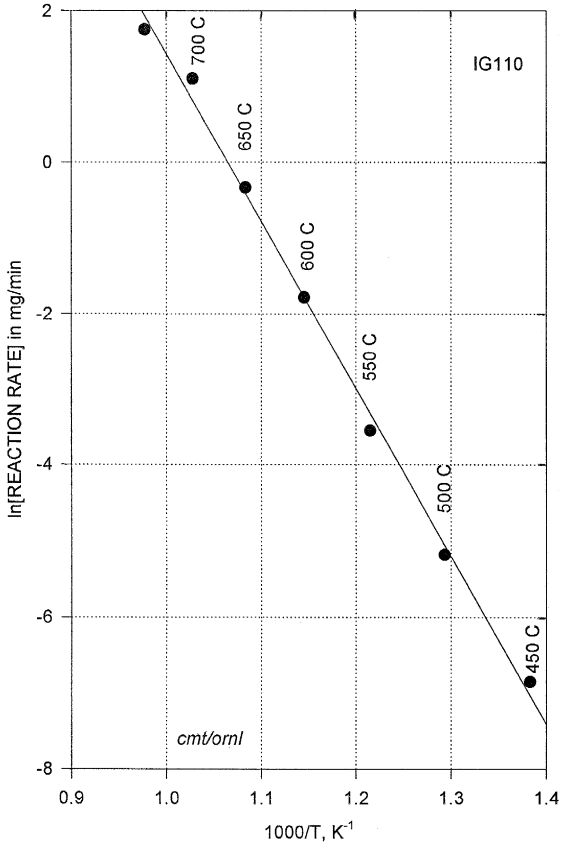

Fig. 4. Temperature effects on the air reaction rate of the graphite cylinders of IG-110. The value of the activation energy (E_a), confirms oxidation reactions are occurring in the Zone II kinetic regime.

Table 6
Rate parameters for the air oxidation of Toyo Tanso IG-110 graphite. Variation with consumption (burn-off) for temperatures 450 to 750°C

Burn-off (%)	ln A	E_a/R	R squared
5.57	24.58	23.53	0.993
13.30	23.86	22.32	0.998
25.29	23.73	21.20	0.983
42.62	25.30	23.61	0.998
53.88	23.07	21.60	0.990
62.83	25.73	24.27	0.999
77.13	22.92	21.85	0.980

It has been reported in literature that apart from the influence of catalysis, the value of activation energies in the oxygen interaction with graphite reflect the product ratio of CO_2 to CO [10]. The results from our experiments presented in Fig. 5 show a constant value in E_a and the frequency factor A, independent of the degree of burn-off and sample type. A similar observation was noted for H-451 graphite. Experiments are currently underway to determine the CO/CO_2 product ratio at various temperatures. The preexponential factor A was also determined from the absolute rate theory employing Eq. (15) and assuming that the ratio of f^*/f_g is equal to unity [29]. At 750°C, A has a theoretical value of 5.328×10^{10} s^{-1} compared to the experimental value of 3.314×10^{10} s^{-1}. The slightly higher theoretical value is indicative of some loss in the degree of translational freedom of oxygen in the formation of the activated complex. This is confirmed in the negative value -41.40 eu of the entropy that is calculated from the activation energy of the reaction. This magnitude of the entropy change agrees excellently with the value predicted by theory. The entropy of a gaseous molecule of oxygen is contributed to by three degrees of translational freedom, two degrees of rotational freedom and a negligible vibration [30]. Translational contribution can be calculated from the following equations:

$$ {}_2\Delta S^\circ(T) = R \ln(M^{3/2}T^{5/2}) - 2.30 \quad (16) $$

$$ {}_3\Delta S^\circ(T) = R \ln(MTA) + 65.80 \quad (17) $$

where ${}_3\Delta S^\circ(T)$ is the entropy of three degrees of translational freedom for a free gas molecule of weight M at one atmosphere pressure and ${}_2\Delta S^\circ(T)$ is the entropy of two degrees of translational freedom for a gas molecule constrained to move in two dimensions within an area A

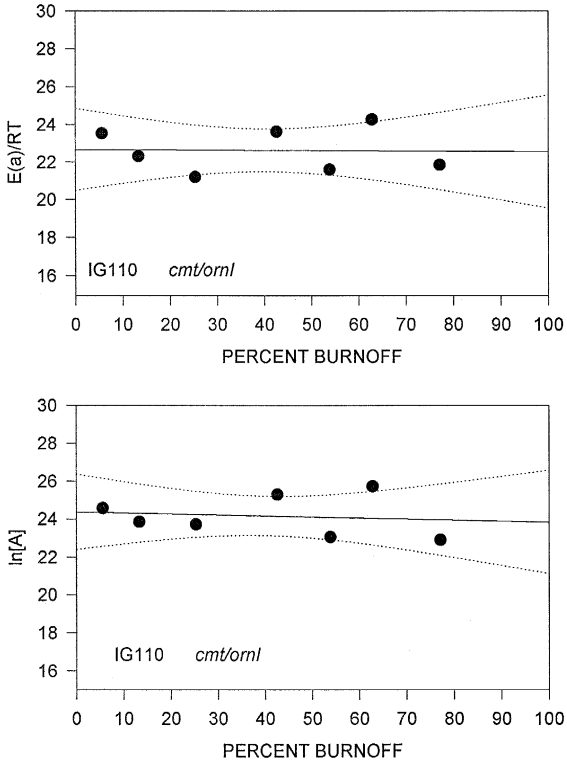

Fig. 5. Regression of thermochemical data for IG-110. Within a 95% confidence level, the activation energy (E_a) and the pre-exponential factor (A) remained essentially constant with fractional burn-off. A common chemical process is in play, with kinetic trends due to induced morphologic variations.

(occupied by two adjacent adsorption sites) on the carbon surface. The rotational contribution is given by

$$S_2 = \ln I + \ln T + 88.59, \quad (18)$$

where I is the moment of inertia of oxygen. The entropy change if all degrees of translational freedom were lost, assuming no change in rotational degree of freedom will be -41 eu. The total entropy change if two degrees of translational freedom and all rotational freedom were lost would be -39 eu, the sum of -23 (trans) and -16 (rot). Both -39 and -41 eu are in close agreement with our value of -41.4 eu. suggesting the adsorption of oxygen through an immobile transition state complex.

4. Conclusions and recommendations

(1) The air oxidation reactions of IG-110 in the temperature range 45 to 750°C and at the low air flow rate of ~ 0.500 SLPM is in pore diffusion controlled.

(2) In a typical air accident scenario, reaction rate becomes diffusion controlled. It is thus recommended that the study of air oxidation of IG-110 be extended into this region.

(3) Air oxidation appears to occur in three stages. A more thorough study of the duration of each stage is needed using larger cylinders of different sizes in order to evaluate maximum rates for the typical large billets that are used in MHTGR.

(4) Structural parametric and fractal analysis establish that the cylinders of IG-110 that were utilized in this study are smooth microporous solids after manufacture. In comparison with H-451, it appear that halogen purification exerts a pronounced effect on binder integrity, making IG-110 more reactive.

(5) The activation energy (E_a) of the reactions reveals that the site of oxidation is on the surface of the pores. The evaluation of the initial rates of reaction which occurs in micropores may be used to characterize the surface property of each cylinder immediately after manufacture.

(6) The activation energy (E_a) and pre-exponential factor remained constant with burn-off in the temperature range studied. However, a more thorough evaluation of the effect of the level of impurities on E_a is desirable. This may be accomplished by doping IG-110 to different levels of impurity and studying the effect on oxidation.

References

[1] G. Haag, D. Minderman, G. Wilhem, H. Persicke and W. Ulsamer, J. Nucl. Mater. 171 (1990) 41.
[2] E.L. Fuller Jr. and B.R. Chilcoat, Graphite Corrosion Kinetics and Mechanisms: Rate Data, DOE-HTGR-88462, ORNL/GCR-90/2.
[3] E.L. Fuller Jr., O.C. Kopp and A.D. Underwood, 'Kinetic and mechanisms of graphite oxidation: a microgravimetric system for evaluation of chemical and structural effects', Proc. 20th Conf. on Carbon (American Carbon Society, June 1991) p. 604.
[4] M.B. Richards, Energy 15 (1990) 729.
[5] H. Marsh, Introduction to Carbon Science (Butterworths, London, 1989) p. 133.
[6] J.L. Su and D.D. Perlmuter, AICHE J. 31 (1985) 6.
[7] D. Farin and D. Avnir, in: The Fractal Approach to Heterogeneous Chemistry, ed. D. Avnir (Wiley, New York, 1989) p. 271.
[8] D. Farin and D. Avnir, in: The Fractal Approach to Heterogeneous Chemistry, ed. D. Avnir (Wiley, New York, 1989) p. 273.
[9] P. David, C. Fung, C. Fairbridge and R. Anderson, Fuel 67 (1988) 755.
[10] J.B. Lewis, Thermal Gas Reactions of Graphite, Modern Aspects of Graphite Technology, ed. L.C.F. Blackman (Academic Press, New York, 1970) p. 139.
[11] C. Heuchamps and X. Duval, Carbon 4 (1966) 243.
[12] L.K. Doraiswamy and M.M. Sharma, Heterogeneous Reactions: Analysis, Examples and Reactor Design, Vol. 1 (Wiley, New York, 1983) p. 17.
[13] P. Hawtin and R. Murdoch, Chem. Eng. Sci. (1964) 819.
[14] N.R. Laine, F.J. Vastola and P.L. Walker Jr., J. Phys. Chem. 67 (1963) 31963.

[15] P.L. Walker, Jr., L.G. Austin and J.J. Tietjen, Chemistry and Physics of Carbon, Vol. 1 (Dekker, New York, 1965) pp. 322–365.
[16] J. Glasstone, K.J. Laidler and H. Eyring, The Theory of Rate Processes (McGraw Hill, New York, 1941).
[17] P.L. Walker Jr., Carbon 24 (1986) 379.
[18] E.E. Peterson, P.L. Walker Jr. and C.C. Wright, Ind. Eng. Chem. 47 (1955) 1629.
[19] M. Kawahata and P.L. Walker Jr., PhD thesis, submitted by M. Kawahata to the Graduate School of the Pennsylvania State University, (Jan. 1960).
[20] L.E. Cascarini De Torre, J.L. Leanos and E.J. Bottani, Carbon 29 (1991) 1051.
[21] G.Q. Lu and D.D. Do, Carbon 29 (1991) 207.
[22] G. Blyholder and H. Eyring, J. Phys. Chem. 61 (1957) 682.
[23] P. Hawkin, J.A. Gibson and R.A. Huber, Carbon 6 (1968) 901.
[24] E.L. Evans and J.M. Thomas, Proc. 3rd Industrial Carbon and Graphite Conf., ed. J.G. Gregory (Society of Chemical Industry, London, 1971) p. 3.
[25] R.T.K. Baker and P.S. Harris, Carbon 11 (1973) 25.
[26] P.L. Walker, Jr., R.L. Taylor and J.M. Ranish, Carbon 29 (1991) 411.
[27] D. Avnir and D. Farin, J. Chem. Phys. 79 (1983) 3566.
[28] M.A. Nay and J.L. Morrison, Can. J. Res. 27 (1948) 205.
[29] J.F. Strange and P.L. Walker Jr., Carbon 14 (1976) 345.
[30] R.O. Lussow, F.J. Vastola and P.L. Walker Jr., Carbon 5 (1967) 591.